Hindawi
Journal of Chemistry
Volume 2020, Article ID 5868174, 12 pages
https://doi.org/10.1155/2020/5868174

Research Article

Kinetic Analysis of the Reduction Processes of a Cisplatin Pt(IV) Prodrug by Mesna, Thioglycolic Acid, and Thiolactic Acid

Yanqing Xia,[1] Hongwu Tian,[2,3] Yanlei Li,[2,3] Xinru Yang,[2,3] Jinming Liu,[2,3] Chunli Liu,[1] Li Zhou,[1] Lincai Zhang,[1] Tiejian Li,[2,3] and Tiesheng Shi[1]

[1]*College of Chemistry, Chemical Engineering and Materials Science, Zaozhuang University, Zaozhuang 277160, Shandong Province, China*
[2]*National Engineering Technology Center of Chirality Pharmaceuticals, Lunan Pharmaceutical Group Co., Ltd., Linyi 276006, Shandong Province, China*
[3]*Shandong New Time Pharmaceutical Co., Ltd., Feixian 273400, Shandong Province, China*

Correspondence should be addressed to Tiejian Li; litiejian@lunan.cn and Tiesheng Shi; rock@uzz.edu.cn

Received 26 July 2020; Revised 23 September 2020; Accepted 15 October 2020; Published 12 November 2020

Academic Editor: Claudia Crestini

Although Mesna is an FDA-approved chemotherapeutic adjuvant and an antioxidant based largely on its antioxidative properties, kinetic and mechanistic studies of its redox reactions are limited. A kinetic analysis of the reduction processes of *cis*-diamminetetrachloroplatinum(IV) (*cis*-$[Pt(NH_3)_2Cl_4]$, a cisplatin Pt(IV) prodrug) by thiol-containing compounds Mesna, thioglycolic acid (TGA), and DL-thiolactic acid (TLA) was carried out in this work at 25.0°C and 1.0 M ionic strength. The reduction processes were followed under pseudo-first-order conditions and were found to strictly obey overall second-order kinetics; the observed second-order rate constant k' versus pH profiles were established in a wide pH range. A general reaction stoichiometry of $\Delta[\text{Pt(IV)}] : \Delta[\text{Thiol}]_{\text{tot}} = 1 : 2$ was revealed for all the thiols; the thiols were oxidized to their corresponding disulfides which were identified by mass spectrometry. Reaction mechanisms are proposed which involves all the prololytic species of the thiols attacking the Pt(IV) prodrug in parallel, designating as the rate-determining steps. Transient species chlorothiol and/or chlorothiolate are formed in these steps; for each particular thiol, these transient species can be trapped rapidly by another thiol molecule which is in excess in the reaction mixture, giving rise to a disulfide as the oxidation product. The rate constants of the rate-determining steps were elucidated, revealing reactivity enhancements of $(1.4–8.9) \times 10^5$ times when the thiols become thiolates. The species versus pH and reactivity of species versus pH distribution diagrams were constructed, demonstrating that the species $^-SCH_2CH_2SO_3^-$ of Mesna largely governs the total reactivity when pH > 5; in contrast, the form of Mesna *per se* (mainly as $HSCH_2CH_2SO_3^-$) makes a negligible contribution. In addition, a well-determined dissociation constant for the Mesna thiol group ($pK_{a2} = 8.85 \pm 0.05$ at 25.0°C and $\mu = 1.0$ M) is offered in this work, which was determined by both kinetic approach and spectrophotometic titration method.

1. Introduction

Mesna (namely, sodium 2-mercaptoethanesulfonate) is an FDA-approved drug which has been used to reduce the risk of hemorrhagic cystitis (a condition that causes inflammation of the bladder and can result in serious bleeding) in people who receive ifosfamide or cyclophosphamide for cancer treatments [1–3]. These two anticancer drugs *in vivo* may be converted to urotoxic metabolites such as acrolein. The protecting mechanism of Mesna is assisting to detoxify these metabolites by reaction of its thiol group with the α,β-unsaturated carbonyl containing compounds including acrolein. Thus, Mesna is a chemotherapeutic adjuvant [1–3]. Moreover, it is also an antioxidant, and its FDA approval was based largely on its antioxidative properties [1–3]. On the other hand, the protonated form of Mesna is 2-mercaptoethanesulfonic acid which bears another name: coenzyme M [4–7]. Coenzyme M is the smallest known organic cofactor and serves as a methyl group carrier in key reactions within the pathway of methane formation from C1

precursors [6]. In the alkene metabolism pathway, it is involved in aliphatic epoxide carboxylation [4–7].

Cisplatin (*cis*-$[Pt(NH_3)_2Cl_2]$), the first Pt(II)-based antineoplastic drug, has played a central role in cancer chemotherapies covering a relatively wide spectrum including testicular, ovarian, cervical, breast, bladder, head and neck, esophageal and lung cancers, mesothelioma, brain tumors, and neuroblastoma [8–10]. Despite of its tremendous success, it has several severe side effects such as nephrotoxicity, ototoxicity, neurotoxicity, and gastrointestinal toxicity in addition to the acquired resistance to the drug [9, 10]. Two general approaches have been developed in order to overcome or minimize these detrimental side effects [11]: (a) the search of adjuvant or rescuing agents which are used together with cisplatin [12–14], and (b) the conversation of cisplatin to its Pt(IV) prodrugs by assumption that these prodrugs can be delivered to the tumor sites more efficiently [15–18]. The first approach has had a very limited success, as such, Mesna has been found to ameliorate significantly the severe side effects of cisplatin in certain types of cancers [19–23]. Furthermore, the combined use of cisplatin, ifosfamide, and Mesna has been exploited to the treatment of advanced ovarian carcinoma [24–26]. Whereas the second approach still remains elusive although large efforts have been attempted [11]. Also, it was shown that cisplatin Pt(IV) prodrugs can induce oxidative stress [18]; this might be not surprising since Pt(IV) prodrugs *per se* are oxidants.

In contrast to the rich biomedical studies of Mesna, the kinetic and mechanistic aspect related to the redox reactions is scanty [27–29], which encompasses the interaction of Mesna with cisplatin [27] and the reduction reactions of bromate and bromine [28] and of the anticancer prodrug ruthenium(III) compound [29] by Mesna. We carried out a kinetic analysis of the reduction processes of *cis*-diamminetetrachloroplatinum(IV) (*cis*-$[Pt(NH_3)_2Cl_4]$) by Mesna and its structurally related thiols thioglycolic acid (TGA) and DL-thiolactic acid (TLA), *cf.* their structures in Figure 1. *cis*-$[Pt(NH_3)_2Cl_4]$ *per se* is anticancer active [30, 31] and is also a prodrug of cisplatin since it is usually reduced to cisplatin. The essentially substitution-inertness property of *cis*-$[Pt(NH_3)_2Cl_4]$ enabled us to study its redox reactions in a wide pH range and to derive the reactivity of each protolytic species of reductants [32, 33]. We thus divulge the results from the kinetic analysis.

2. Materials and Methods

2.1. Chemicals. Mesna, thioglycolic acid, DL-thiolactic acid, the platinum(IV) compound *cis*-$[Pt(NH_3)_2Cl_4]$, and *cis*-$[Pt(NH_3)_2Cl_2]$ (cisplatin) were purchased from Sigma-Aldrich (St. Louis, MO). Phosphoric acid, acetic acid, sodium acetate, sodium dihydrogen phosphate, disodium hydrogen phosphate, sodium carbonate, sodium bicarbonate, sodium perchlorate, perchloric acid, sodium chloride, and Na_2EDTA in their purist forms available were obtained from either Fisher Scientific or Alfa Aesar which were used to prepare buffer solutions. All the solutions were prepared by use of doubly distilled water.

2.2. Instruments. UV-Vis spectra, absorption measurements, and time-resolved spectra were recorded on a TU-1900 spectrophotometer (Beijing Persee, Inc., Beijing, China) using 1.00 cm quartz cells. Kinetic measurements and rapid scan spectra were carried out on an Applied Photophysics SX-20 stopped-flow spectrometer (Applied Photophysics Ltd., Leatherhead, U.K.). Both spectrophotometer and spectrometer were equipped with a water bath circulation from a thermostat (Lauda Alpha RA8, Belran, NJ, USA); temperature could be controlled to $\pm 0.1^{\circ}C$. Mass spectra were recorded on an Agilent 1200/6310 ion trap mass spectrometer with electrospray ionization (ESI). An Accumet Basic AB15 Plus pH meter, equipped with an Accumet AccutupH® combination pH electrode (Fisher Scientific, Pittsburgh, PA), was used to measure the pH values of buffer solutions. Standard buffers of pH 4.00, 7.00, and 10.00, also from Fisher Scientific, were used for calibrations of the electrode just before pH measurements.

2.3. Buffer Solutions. Buffering pairs of H_3PO_4/NaH_2PO_4, HAc/NaAc, NaH_2PO_4/Na_2HPO_4, $NaHCO_3/Na_2CO_3$, and Na_2HPO_4/Na_3PO_4 (0.15–0.2 M) were prepared to cover a pH range from $2.47 \leq pH \leq 11.97$. The buffers contained 0.10 M of NaCl and 2.0 mM of EDTA; sodium perchlorate was used to adjust the ion strength (μ) of buffers to an ionic strength of 1.0 M. Details for the buffer preparations are delineated in our earlier works [32, 33]. The buffer pairs are listed in Table S1 in the Supplementary Materials (SM).

2.4. Kinetic Experiments. Stock solutions of 1.0 mM *cis*-$[Pt(NH_3)_2Cl_4]$ were daily prepared by dissolving the desired amount of *cis*-$[Pt(NH_3)_2Cl_4]$ in a solution containing 0.90 M $NaClO_4$, 0.09 M NaCl, and 0.01 M HCl; these solutions were only used for a couple of hours. Stock solutions of thiols were prepared by adding the needed amount of the thiol to a buffer solution of specific pH. The solutions were flushed with highly pure nitrogen gas for 10 min. Solutions of Pt(IV) and thiol for kinetic measurements were prepared by dilution of the stock solutions with the same pH buffer and were then nitrogen-flushed for 10 min before loading onto the stopped-flow spectrometer. Equal volumes of Pt(IV) and thiol solutions were mixed directly in the stopped-flow instrument. Kinetic traces were followed between 265 and 280 nm; pseudo-first-order conditions were fulfilled with a 10-fold excess of $[thiol]_{tot}$ over [Pt(IV)], where $[thiol]_{tot}$ represents the total concentration of thiol.

2.5. Stoichiometric Measurements. For each of the thiols, a series of reaction mixtures were prepared in a phosphate buffer of pH 6.25 in which [Pt(IV)] = 0.30 mM was retained constant whereas $[thiols]_{tot}$ was changed from 0 to 1.50 mM. For each of the reaction mixtures, the absorption values at 265 nm were determined after a reaction time of 8–10 min at room temperature.

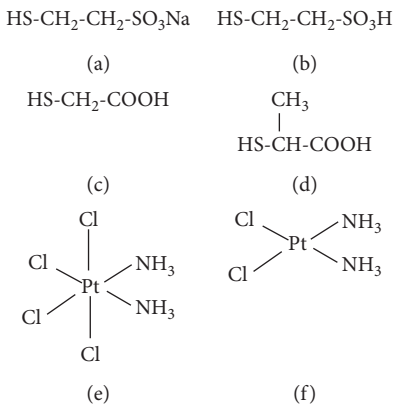

Figure 1: Structures of thiol-containing compounds: (a) Mesna (sodium 2-mercaptoethane-sulfonate), (b) coenzyme M (2-Mercaptorthanesulfonic acid), (c) thioglycolic acid (TGA), (d) thiolactic acid (TLA), (e) *cis*-$[Pt(NH_3)_2Cl_4]$, and (f) *cis*-$[Pt(NH_3)_2Cl_2]$ (cisplatin).

3. Results and Discussion

3.1. UV-Vis and Rapid-Scan Spectra. The UV-Vis spectra for the compounds employed in this work were recorded by use of their solutions freshly prepared in a buffer of pH 4.42. The obtained spectra for 0.20 mM *cis*-$[Pt(NH_3)_2Cl_4]$, 0.20 mM *cis*-$[Pt(NH_3)_2Cl_2]$, 1.0 mM Mesna, 1.0 mM TGA, and 1.0 mM TLA are shown in the upper panel of Figure S1. In addition, the UV-Vis spectra for the fresh solutions of 0.20 mM *cis*-$[Pt(NH_3)_2Cl_4]$ in buffers of pH 4.42, 6.67, and 10.98 were also recorded, and are given in the lower panel of Figure S1.

In order to gain some insights into these reduction processes, the reduction of *cis*-$[Pt(NH_3)_2Cl_4]$ by Mesna in a buffer of pH 6.25 was probed by recording the rapid scan spectra under a set of reaction conditions. The spectra were recorded between 200–350 nm and are shown in Figure 2(a). Clearly, the absorption band around 236 nm and absorption shoulder round 265 nm decreased concertedly as the reaction proceeded, and no new absorption bands emerged. The absorbance readings at 236 and 266 nm as a function of time are shown in Figure 2(b) (data points). The absorbance versus time curves or kinetic traces were fit by equation (1) [34], where k_{obsd} represents of pseudo-first-order rate constant and

$$A_t = (A_0 - A_\infty)\exp(-k_{obsd}) + A_\infty, \quad (1)$$

where A_t, A_0, and A_∞ pertain to absorbance at time t, zero, and infinity, respectively. The resulting fittings are excellent (Figure 2(b)) and moreover, the value of k_{obsd} obtained at 236 nm equals to that acquired at 266 nm within the experimental errors. These kinetic attributes indicate that the reduction process is first-order in [Pt(IV)] and that the absorbance decrease in Figure 2 corresponds to the reduction of *cis*-$[Pt(NH_3)_2Cl_4]$ without other complications. As a matter of fact, the kinetic attributes are in good agreement with the nature of substitution inertness of Pt(IV) complexes in general [35, 36]. In the time-resolved spectra recorded for the reduction process of *cis*-$[Pt(NH_3)_2Cl_4]$ by TLA in an acidic medium, similar spectral and kinetic attributes were observed, *cf*., Figure S2 in the SM.

3.2. Second-Order Kinetics and Data Collection. The effects of varying $[thiol]_{tot}$ on the reduction rates were studied, aiming at ascertaining the reaction order of the thiols. In most of buffer solutions, $[thiol]_{tot}$ was varied from 0.20 to 2.00 mM and the reaction medium had big enough buffering capacities so that the variation of $[thiol]_{tot}$ did not cause any pH changes in the medium. The kinetic traces were followed by the stopped-flow spectrometer in a wavelength region from 265 to 280 nm. Pseudo-first-order rate constant k_{obsd} was acquired from the simulations of kinetic traces by equation (1). For each $[thiol]_{tot}$, 3–5 duplicate runs were made, and the values of k_{obsd} were the averages from the duplicated runs. Standard deviations are usually much less than 5%.

Plots of k_{obsd} versus $[thiol]_{tot}$ in the case of Mesna are shown in Figure 3 for a series of buffers at 25.0°C and 1.0 M ionic strength ($\mu = 1.0$ M). Similar plots for the reactions of TGA and TLA are shown in Figures S3 and S4 in the SM. Undoubtedly, all the plots in Figures 3, S3, and S4 are linear and do not have any significant intercepts. Thus, the reduction reactions are first-order in $[thiol]_{tot}$; thus, an overall second-order rate law (2) is warranted, where k' denotes the observed second-order rate constant and $k' = k_{obsd}/[thiol]_{tot}$:

$$-\frac{d[Pt(IV)]}{dt} = k_{obsd}[Pt(IV)] = k'[thiol]_{tot}[Pt(IV)]. \quad (2)$$

We collected a large body of kinetic data at 25.0°C and $\mu = 1.0$ M covering a wide pH range. Values of k' were calculated from the linear k_{obsd} versus $[thiol]_{tot}$ plots for all the three thiols and are summarized in Tables S1–S3 in the SM. Alternatively, $\log k'$ versus pH plots are illustrated in Figures 4 and 5 (data points).

3.3. Reaction Stoichiometry and the Oxidation Products. A spectrophotometric titration method was employed to find the stoichiometry for the redox reactions between *cis*-$[Pt(NH_3)_2Cl_4]$ and the thiols [32–34]. The plots of absorption values at 265 nm versus the ratio $[thiol]_{tot}/[Pt(IV)]$ are displayed in Figure 6. For each thiol, the data points clearly follow two crossing straight lines affording an intersection point. The stoichiometric ratios were acquired

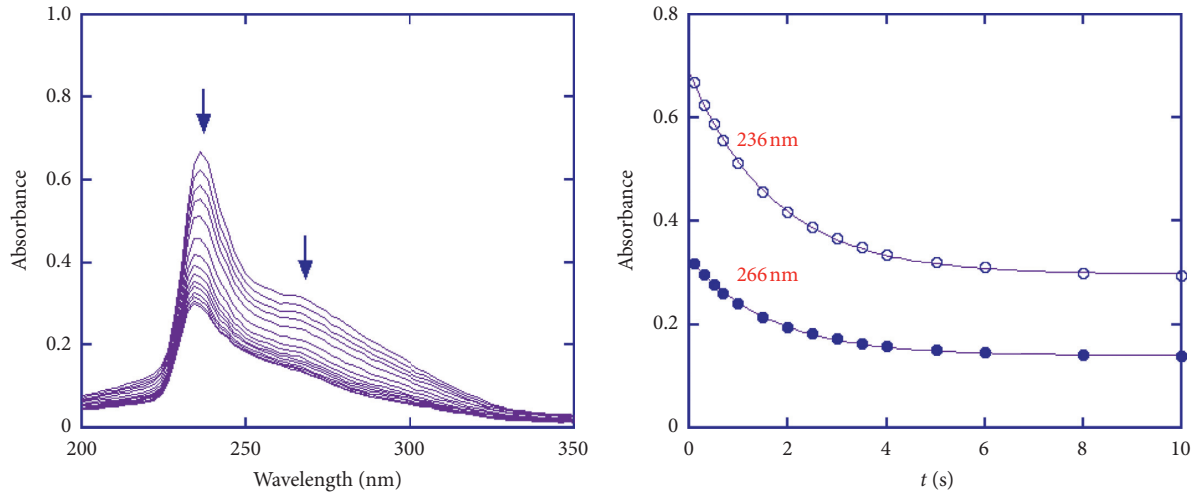

FIGURE 2: (a): Rapid scan spectra acquired for the reduction of *cis*-$[Pt(NH_3)_2Cl_4]$ by Mesna under a set of reaction conditions: [Pt(IV)] = 0.10 mM, $[Mesna]_{tot}$ = 1.00 mM, phosphate buffer of pH 6.25, 25.0°C, and μ = 1.0 M. The spectra were acquired at 0.10, 0.30, 0.50, 0.70, 1.0, 1.5, 2.0, 2.5, 3.0, 3.5, 4.0, 5.0, 6.0, 8.0, and 10.0 seconds after start of the reaction. (b): Kinetic traces at 236 and 265 nm (data points) from the rapid scan spectra; the solid-curves were the best fits of equation (1) to the experimental data by a nonlinear squares method, providing values of $k_{obsd} = 0.58 \pm 0.02\ s^{-1}$ at 236 nm and $0.61 \pm 0.02\ s^{-1}$ at 266 nm.

from these intersection points: 1.81 ± 0.05 for TGA, 1.87 ± 0.05 for TLA, and 1.97 ± 0.05 for Mesna. These ratios, within the experimental errors, point virtually to a reaction stoichiometry of $\Delta[Pt(IV)] : \Delta[Thiol]_{tot} = 1 : 2$. Stoichiometric reaction (3a) is thus suggested for the reactions of TGA (R = H) and TLA (R = Me), while the stoichiometric reaction (3b) is inferred for the Mesna reaction where the sulfonic acid groups are deprotonated due to its strong acidity (vide infra):

$$[Pt(NH_3)_2Cl_4] + 2HSCHRCOOH \longrightarrow [Pt(NH_3)_2Cl_2] + HOOCCHRSSCHRCOOH + 2HCl \quad (3a)$$

$$[Pt(NH_3)_2Cl_4] + 2HSCH_2CH_2SO_3^- \longrightarrow [Pt(NH_3)_2Cl_2] + {}^-O_3SCH_2CH_2SSCH_2CH_2SO_3^- + 2HCl \quad (3b)$$

ESI mass spectra were recorded for reaction mixtures of 1 mM Pt(IV) with 8 mM TGA and of 1.0 mM Pt(IV) with 8 mM TLA in 10 mM HCl after a reaction time about 1 h; the obtained spectra are shown in Figures S5 and S6 in the SM together with the peak assignments. From the peak assignments, formations of disulfides $HOOCCH_2S$-SCH_2COOH and HOOCCMeS-SCMeCOOH were confirmed for the reactions of TGA and TLA, respectively.

3.4. Reaction Mechanisms. The observed second-order rate constants k' increase several orders of magnitude (Table S1–S3 and Figures 4 and 5) when the reaction media are changed from acidic via neutral to basic for the three thiols, unveiling that the thiolate species of TGA, TLA, and Mesna are much more reactive than their corresponding thiol forms. On the other hand, *cis*-$[Pt(NH_3)_2Cl_4]$ possesses an octahedral configuration; substitution reactions on the Pt(IV) compounds are generally very sluggish [35, 36]. In contrast, the reduction processes of *cis*-$[Pt(NH_3)_2Cl_4]$ by the three thiols are much quicker, thus ruling out the possibility that the reduction reactions proceed via ligand substitution(s). This is consistent with the attributes found in the time-resolved spectra discussed above. If all the protolytic species of TGA, TLA, and Mesna are logically assumed to be able to reduce the Pt(IV) complex, the reaction mechanism delineated in Scheme 1 is suggested for the reactions of TGA and TLA [32, 33]. The reaction mechanism described in Scheme 2 is proposed analogously for the Mesna reaction. In the mechanisms, the reactions designated by k_1–k_3 are the rate-determining steps. Each of the steps is taking place via an attack on one of the two axially-coordinated chlorides by the sulfur atom of the thiols, forming chloride-bridged transitions states which in the case of Mesna are depicted conceivably as follows [37–39]:

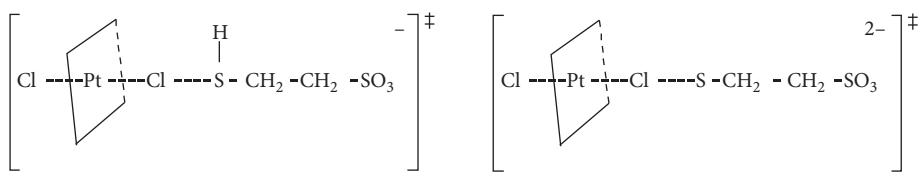

(4)

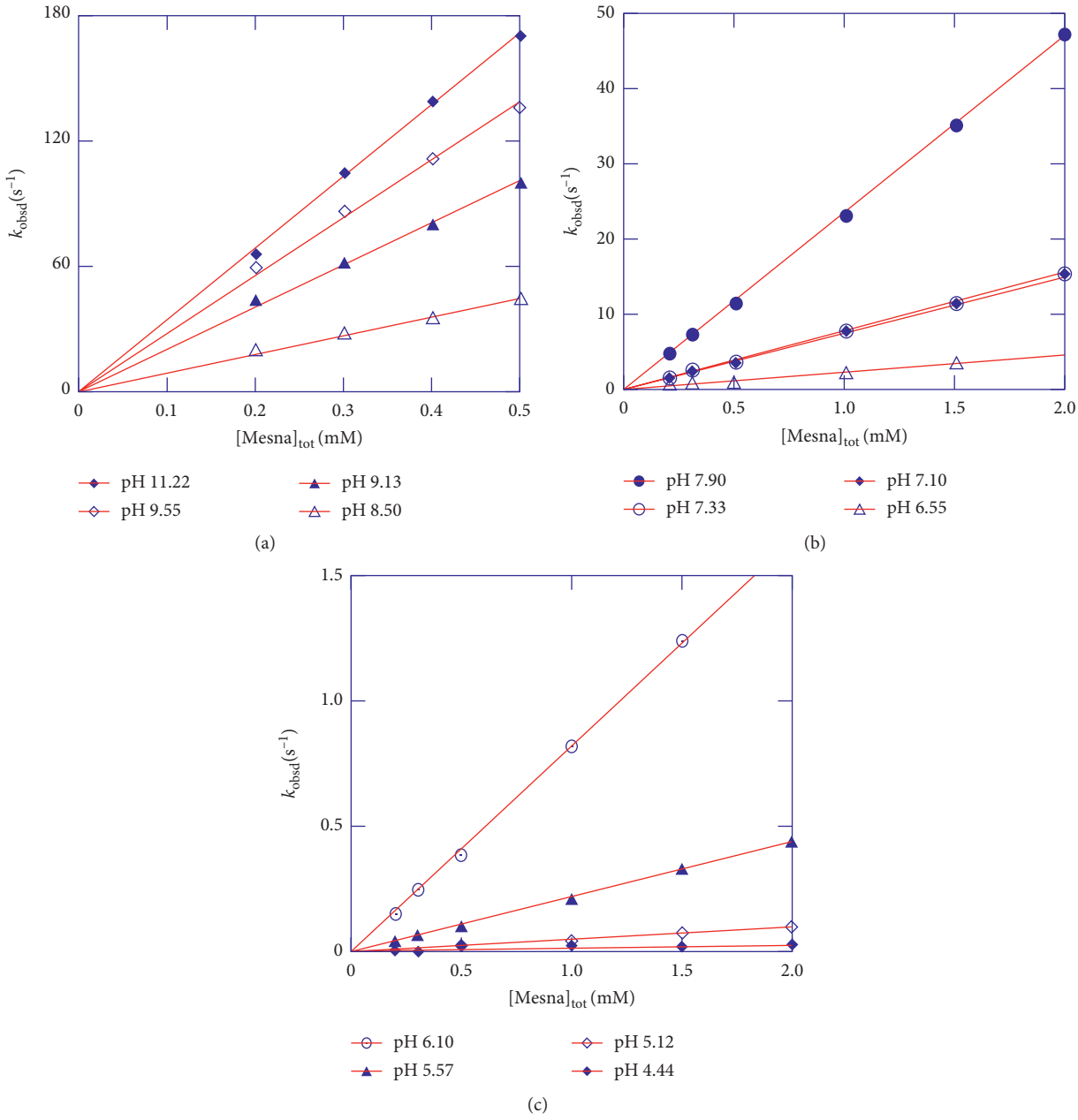

FIGURE 3: Pseudo-first-order rate constants k_{obsd} versus $[Mesna]_{tot}$ in buffer solutions of different pHs at 25.0°C and $\mu = 1.0$ M.

In the transition states, partial bond formation (or bridge formation) between Cl and S atom occurs whereas concurrently the bonds of Cl-Pt-Cl are partially broken [37–39]. The collapses of the transition states generate transient chlorothiol and/or chlorothiolate species [37–39]. For each particular thiol, these transient species can be trapped rapidly by another thiol molecule which is in excess in the reaction mixture, giving rise to a disulfide as the oxidation product [32, 33, 37].

3.5. Rate Constants of the Rate-Determining Steps. The reaction mechanisms outlined in Schemes 1 and 2 are very similar and a common rate expression can be derived as follows:

$$-\frac{d[Pt(IV)]}{dt} = \frac{k_1 a_H^2 + k_2 K_{a1} a_H + k_3 K_{a1} K_{a2}}{a_H^2 + K_{a1} a_H + K_{a1} K_{a2}} = [\text{thiol}]_{tot}[\text{Pt(IV)}]. \quad (5)$$

Equation (5) is equivalent virtually to equation (2), where a_H is the proton activity and corresponds to the measured pH values by a relation: $pH = -\log(a_H)$. A comparison of equations (2) and (5) renders

$$k' = \frac{k_1 a_H^2 + k_2 K_{a1} a_H + k_3 K_{a1} K_{a2}}{a_H^2 + K_{a1} a_H + K_{a1} K_{a2}}. \quad (6)$$

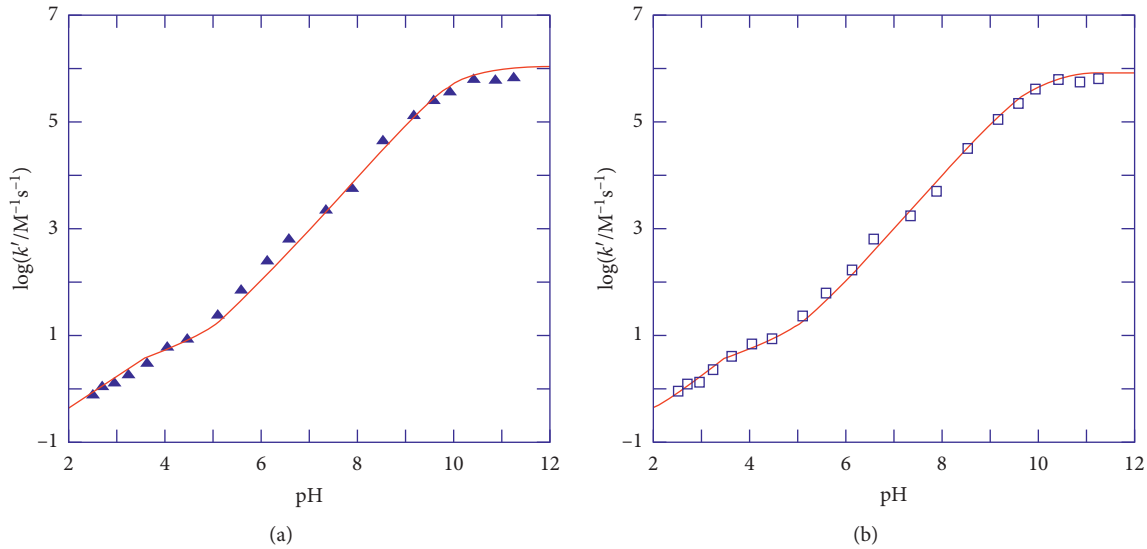

Figure 4: Second-order rate constants k' in logarithmic scale versus pH profiles for (a) TGA and (b) TLA (data points). The solid lines were obtained by simulations of equation (6) to the experimental data by use of a weighted nonlinear least-squares method.

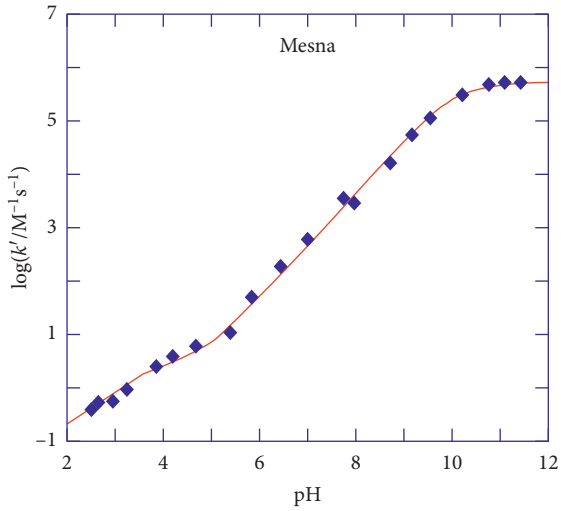

Figure 5: Second-order rate constants k' in logarithmic scale versus pH profile for Mesna (data points). The solid lines were obtained by simulations of equation (7) to the experimental data by use of a weighted nonlinear least-squares method.

Equation (6) was utilized to simulate the kinetic data in Figures 4 and 5. In the simulations, the rate constants k_1–k_3 were unknowns and treated as adjustable parameters. On the other hand, if the acid dissociation constants K_{a1} and K_{a2} for the thiol-containing compounds are available at the relevant conditions, they will be used as direct inputs, minimizing the number of adjustable parameters. Fortunately, the acid dissociation constants of TGA were reported to be $pK_{a1} = 3.53$ and $pK_{a2} = 10.05$ at 25.0°C and $\mu = 1.0$ M [37]. When these pK_a values were used direct inputs, equation (6) was employed to simulate the k'–pH dependence data by use of a weighted nonlinear least-squares method. The simulated result for TGA turned out to be good and is shown in Figure 4(a), concurrently providing values for the rate constants of k_1–k_3 which are listed in Table 1.

The acid dissociation constants of TLA were reported as $pK_{a1} = 3.38$ and $pK_{a2} = 9.93$ at 25.0°C and $\mu = 0.50$ M [40] and were also utilized as direct inputs although the ionic strength is slightly differentiated. The simulation of equation (6) to the k'–pH dependence data revealed an essentially perfect fit, as shown in Figure 4(b). The acquired values of k_1–k_3 from the simulation are also listed in Table 1.

A reliable value of the thiol dissociation constant for Mesna (i.e. pK_{a2} in Scheme 2) appears nonavailable in the literature under our experimental conditions except that some articles [2, 41] mentioned a value of 9.2 without specifying any conditions, which is in contrast to the fact that Mesna has been subjected to extensive medical studies as illustrated in the introduction section. The pK_{a1} value of coenzyme M in Scheme 2 was not found in the literature.

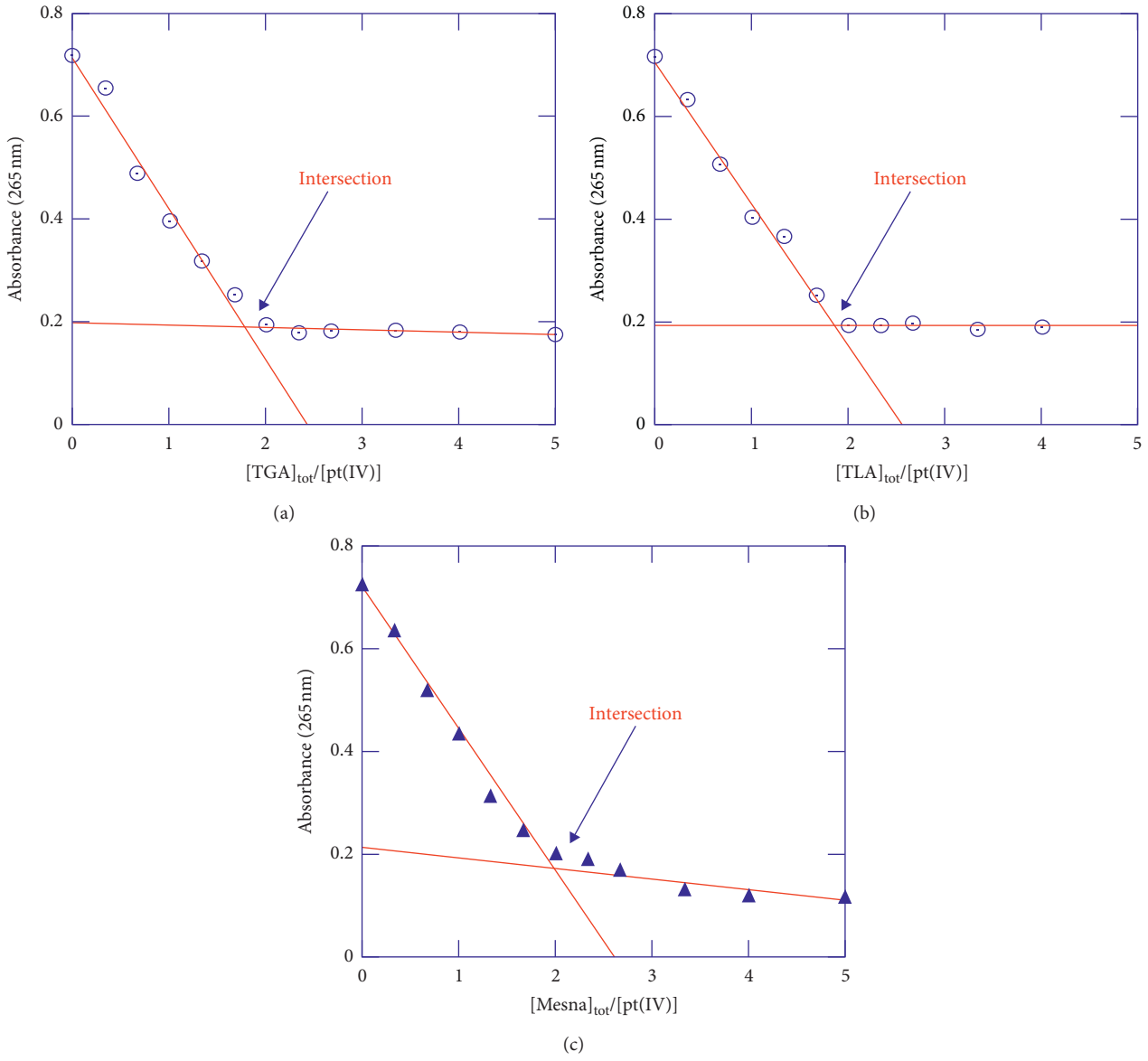

FIGURE 6: Stoichiometric ratios determined by spectrophotometric titrations: absorption values at 265 nm as a function of the ratio $[\text{thiol}]_{\text{tot}}/[\text{Pt(IV)}]$. The intersection points in figure give rise to the stoichiometric values. (a) TGA. (b) TLA. (c) Mensa.

Due to the biomedical importance of Mesna, acquiring a reliable value of the thiol dissociation constant is appealing. On the other hand, the pK_{a1} value of coenzyme M is anticipated to be close to that of ethanesulfonic acid ($CH_3CH_2SO_3H$), which was reported to be $pK_a = 1.65$ at 25.0°C [42].

For the kinetic data analysis by equation (6), an initial value of $pK_{a1} = 1.65$ and a tunable pK_{a2} were tried for the simulations. The trial simulations indicated that the k_1 value was indeterminate when pK_{a1} was varied from 1.2 to 2.0. Thus, the k_1-term in equation (6) is negligible, leading to follows:

$$k' = \frac{k_2 K_{a1} a_H + k_3 K_{a1} K_{a2}}{a_H^2 + K_{a1} a_H + K_{a1} K_{a2}}. \quad (7)$$

Equation (7) was then employed for simulation of the k'-pH dependence data, and the simulated result is shown in Figure 5, conferring well-defined values for $pK_{a2} = 8.86 \pm 0.08$ and $k_3 = (3.29 \pm 0.09) \times 10^5\ \text{M}^{-1}\text{s}^{-1}$ at 25.0°C and $\mu = 1.0$ M. Furthermore, more simulations were performed with pK_{a1} values changed from 1.2 to 2.0 (the real pK_{a1} value is certainly in this region), yielding the robust values for pK_{a2} and k_3 mentioned above. The obtained k_2 values has a small variation, but only changed from 0.32 ± 0.03 to $0.42 \pm 0.03\ \text{M}^{-1}\text{s}^{-1}$. The results are given in Table 1 where k_2 value is taken as an average. Therefore, although the pK_{a1} value of coenzyme M is not known, we obtained the well-defined values for pK_{a2} and k_3, and a reasonable value for k_2.

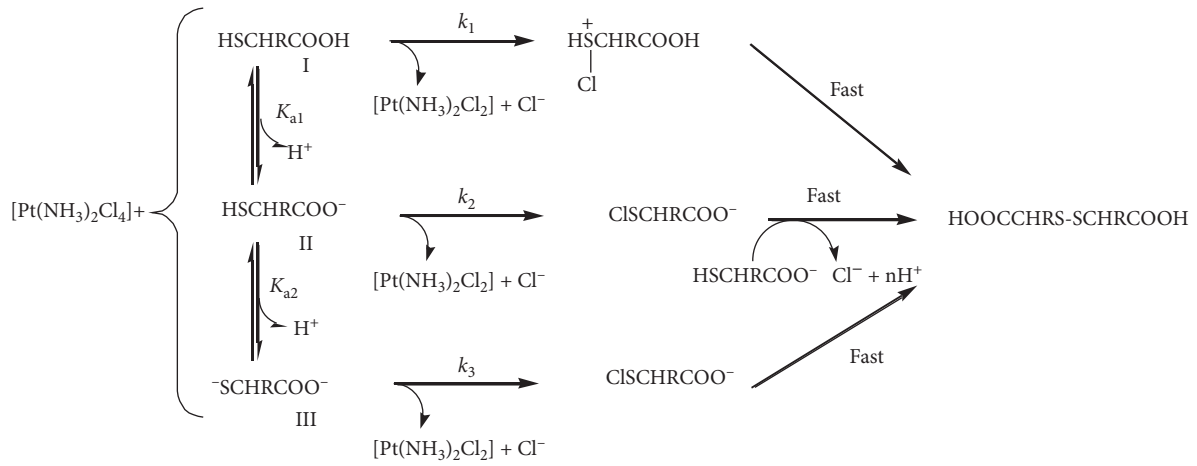

For TGA, R = H; for TLA, R = Me

Scheme 1: A reaction mechanism suggested for the reduction processes of *cis*-$[Pt(NH_3)_2Cl_4]$ by TGA and TLA.

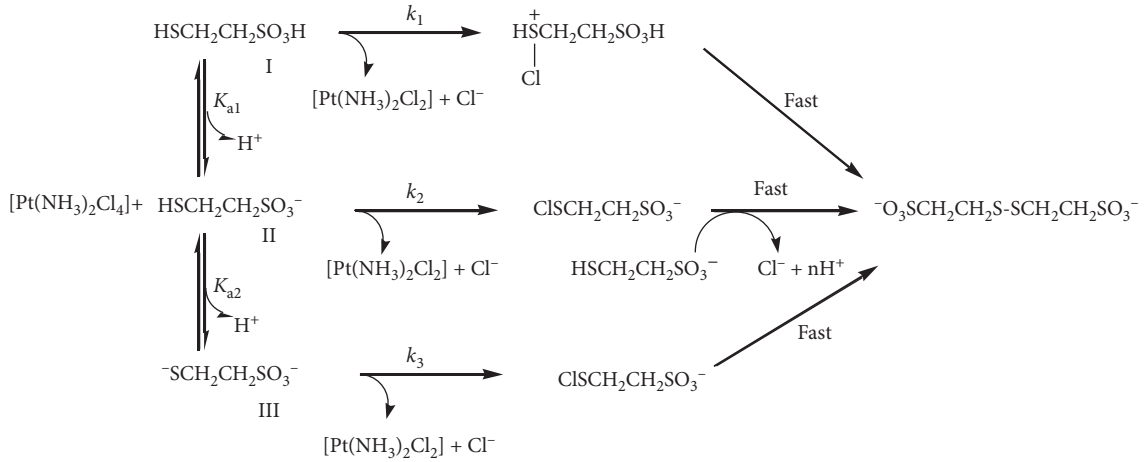

Scheme 2: A reaction mechanism proposed for the reduction process of *cis*-$[Pt(NH_3)_2Cl_4]$ by coenzyme M/Mesna.

3.6. Determination of the Thiol Dissociation Constant of Mesna. In order to further ascertain the pK_{a2} value of Mesna obtained by the above kinetic approach, we thus determined it by the spectrophotometric titration method [43–45]. A series of buffer solutions containing 0.12 mM Mesna at 1.0 M ionic strength were prepared covering a pH range from 6.77 to 11.97. Those solutions were flushed by nitrogen gas and concurrently thermoequilibated at 25.0°C for 10 min. For each pH, absorbance at 235 nm was measured with the corresponding buffer without Mesna as a reference. The measured absorption value as a function of pH is given in Figure 7 (data points). Equation (8) is a standard correction between the measured absorbance and pK_{a2} [43–45] in which ε_2 and ε_3 are the molar absorptivities for $HSCH_2CH_2SO_3^-$ and $^-SCH_2CH_2SO_3^-$,

$$\text{Abs}\,(235\,\text{nm}) = \frac{[\text{Mesna}]_{\text{tot}}\left\{\varepsilon_3 + \varepsilon_2 10^{\left(pK_{a2}-pH\right)}\right\}}{\left\{1 + 10^{\left(pK_{a2}-pH\right)}\right\}}, \quad (8)$$

respectively. The ε_2 value was determined separately to be $59.0 \pm 0.5\ M^{-1}\,cm^{-1}$ by use of three solutions of ca. 10 mM Mesna between pH 4 and 5. Equation (8) was then employed to simulate the data in Figure 7 using a nonlinear least-squares routine; the simulation resulted in a good fit, furnishing $pK_{a2} = 8.85 \pm 0.05$ and $\varepsilon_3 = (5.6 \pm 0.1) \times 10^3\ M^{-1}\,cm^{-1}$ at 25.0°C and $\mu = 1.0$ M. The excellent agreement between the pK_{a2} values obtained by the kinetic approach and by the spectreophotometric titration method emphasizes that we provide a reliable value for Mesna thiol dissociation and that the kinetic approach is a good method for acquisition of pK_a values [46, 47].

Table 1: Values of rate constants derived for the rate-determining steps for reduction of *cis*-$[Pt(NH_3)_2Cl_4]$ by the protolylic species of TGA, TLA, and Mesna at 25.0°C and $\mu = 1.0$ M.

Thiols	pK_a values	k_m	Value ($M^{-1}s^{-1}$)
TGA	$pK_{a1} = 3.53$	k_1	0.26 ± 0.05
	$pK_{a2} = 10.05$	k_2	6.8 ± 0.2
		k_3	$(1.15 \pm 0.05) \times 10^6$
TLA	$pK_{a1} = 3.38$	k_1	0.19 ± 0.04
	$pK_{a2} = 9.93$	k_2	6.2 ± 0.2
		k_3	$(8.8 \pm 0.2) \times 10^5$
Mesna	$pK_{a1} = 1.2$–2.0	k_1	Not obsd.
	$pK_{a2} = 8.86 \pm 0.08$[a]	k_2	0.37 ± 0.09
	$pK_{a2} = 8.85 \pm 0.05$[b]	k_3	$(3.29 \pm 0.09) \times 10^5$

[a]Obtained by kinetic approach. [b]Determined by the spectrophotometric titration method.

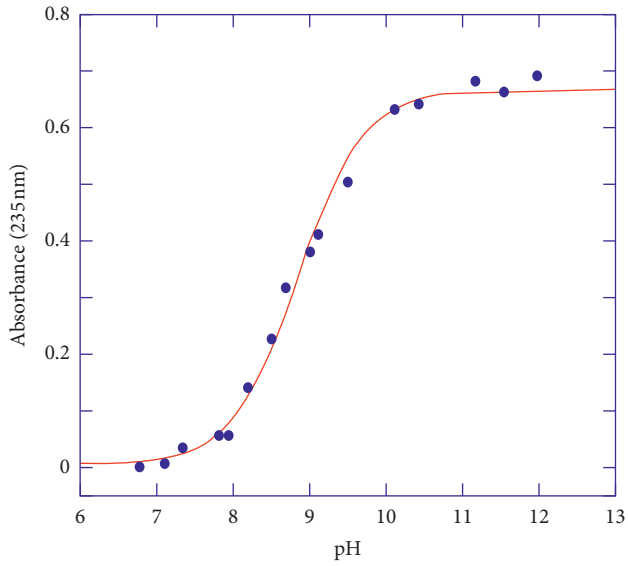

Figure 7: Absorbance at 235 nm of 0.12 mM Mesna solutions as function of pH at 25.0°C and $\mu = 1.0$ M. The solid curve was obtained from the best fit of equation (8) to the experimental data.

3.7. Reactivity of Species the Three Thiols towards the Reduction of cis-$[Pt(NH_3)_2Cl_4]$. Our kinetic data collection in the wide pH range enables us to derive the reactivity of all the protolytic species of the three thiols towards the reduction of *cis*-$[Pt(NH_3)_2Cl_4]$ and to make a comparison. The ratios of $k_1 : k_2 : k_3$ were found to be $0.038 : 1 : 1.7 \times 10^5$ for TGA, $0.031 : 1 : 1.4 \times 10^5$ for TLA, and $0 : 1 : 8.9 \times 10^5$ for coenzyme M (Mesna), respectively. Clearly, the deprotonation of the carboxylic acids in TGA and TLA gives a reactivity enhancement of about 30 times which is caused by an inductive effect conferred by the deprotonations. When the thiols become thiolates after a further deprotonation, reactivity enhancements of $(1.4$–$8.9) \times 10^5$ times are engendered for all the thiols. These huge reactivity enhancements account convincingly for the logk' versus pH profiles in Figures 4 and 5.

More straightforwardly, the species versus pH and the species reactivity versus pH distribution diagrams were constructed [33, 46], which are displayed in Figures S7–S9 in the SM. For all the thiols, species **II** dominate in the existing forms from pH 7.0 to 8.0 but make negligible contributions to their respect total reactivity. On the other hand, species **III** play dominant roles in determining the total reactivity whereas their populations are extremely low in the pH region from 7 to 8. In particular, the protolytic species $^-SCH_2CH_2SO_3^-$ largely dominates the total reactivity of Mesna from above pH 5; contrarily, the form of Mesna *per se* (mainly as $HSCH_2CH_2SO_3^-$) makes a negligible contribution to the total reactivity when pH > 5, *cf.* Figure S10. It follows that the protolytic species $^-SCH_2CH_2SO_3^-$ but not $HSCH_2CH_2SO_3^-$ of Mesna may play a leading role in some pharmacological processes of this drug.

Mechanistically, the reduction processes of *cis*-$[Pt(NH_3)_2Cl_4]$ and of the anticancer model compound *trans*-$[PtCl_2(CN)_4]^{2-}$ [37] by TGA are similar, rendering a possibility of reactivity comparison. The ratios of k_2 ($[PtCl_2(CN)_4]^{2-}$)/k_2 ($[Pt(NH_3)_2Cl_4]$) and k_3 ($[PtCl_2(CN)_4]^{2-}$)/k_3 ($[Pt(NH_3)_2Cl_4]$) were calculated to be 168 and 1.9×10^4, respectively, highlighting that the reduction of *trans*-$[PtCl_2(CN)_4]^{2-}$ is much faster than *cis*-$[Pt(NH_3)_2Cl_4]$. This can be accounted for in terms of transition state stabilization which is ascribed to the strong σ-donor and π-acceptor properties of the cyanide ligands in $[PtCl_2(CN)_4]^{2-}$ [48].

4. Conclusions

The reduction processes of a cisplatin Pt(IV) prodrug *cis*-$[Pt(NH_3)_2Cl_4]$ by Mesna, TGA and TLA strictly follow overall second-order kinetics, and the k' versus pH profiles have been established in a wide pH range. The proposed reaction mechanisms involve all the prololytic species of the thiols attacking the Pt(IV) in parallel, which are the rate-determining steps. The rate constants of these rate-determining steps have been elucidated revealing reactivity enhancements of $(1.4$–$8.9) \times 10^5$ times when the thiols become thiolates. The constructed species versus pH and species reactivity versus pH distribution diagrams demonstrated that the species $^-SCH_2CH_2SO_3^-$ of Mesna largely governs the total reactivity when pH > 5; contrarily, the form of Mesna *per se* (mainly as $HSCH_2CH_2SO_3^-$) makes a negligible contribution. In addition, a well-determined and reliable dissociation constant for the Mesna thiol group

($pK_{a2} = 8.85 \pm 0.05$ at 25.0°C and $\mu = 1.0$ M) is offered in this work.

Data Availability

The data used to support the findings of this study are included within the article.

Conflicts of Interest

The authors declare that there are no conflicts of interest regarding the publication of this paper.

Acknowledgments

Financial support of this work by grants from the Critical R&D Plans of Shandong Province (Major Scientific Innovation Projects, 2019JZZY010516) and from the Natural Science Foundation of Shandong Province (ZR2019MB015) is gratefully acknowledged. The authors thank Dr. Jingran Dong and Mr. Liyao Xu for some experimental assistance.

Supplementary Materials

Table S1: observed second-order rate constants k' for reduction of *cis*-$Pt(NH_3)_2Cl_4$] by thioglycolic acid (TGA) as a function of pH at 25.0°C and 1.0 M ionic strength. Table S2: observed second-order rate constants k' for reduction of *cis*-$Pt(NH_3)_2Cl_4$] by thiolactic acid (TLA) as a function of pH at 25.0°C and 1.0 M ionic strength. Table S3: observed second-order rate constants k' for reduction of *cis*-$Pt(NH_3)_2Cl_4$] by Mesna as a function of pH at 25.0°C and 1.0 M ionic strength. Figure S1 (upper panel): UV-Vis spectra of 0.20 mM *cis*-$[Pt(NH_3)_2Cl_4]$, 0.20 mM *cis*-$[Pt(NH_3)_2Cl_2]$ (cisplatin), 1.0 mM Mesna, 1.0 mM thioglycolic acid (TGA), and 1.0 mM DL-thiolactic acid (TLA) recorded in an HAc/NaAc buffer of pH 4.42. Lower panel: UV-Vis spectra of 0.20 mM *cis*-$[Pt(NH_3)_2Cl_4]$ in buffer solutions of pH 4.42 (HAc/NaAc), pH 6.67 (NaH_2PO_4/Na_2HPO_4), and pH 10.98 (Na_2HPO_4/Na_3HPO_4). For each spectrum, the corresponding buffer was used as a reference. Figure S2 (upper panel): time-resolved spectra acquired for the reduction of *cis*-$[Pt(NH_3)_2Cl_4]$ by TLA under a set of reaction conditions: [Pt(IV)] = 0.07 mM, $[TLA]_{tot} = 1.00$ mM, HAc/NaAc buffer of pH 4.91, 25.0°C, and $\mu = 1.0$ M. The first spectrum was obtained at about 10 seconds after start of the reaction, and the time interval between two adjacent scans was 20 seconds. Lower panel: kinetic traces at 224 nm and 270 nm (data points) from the time-resolved spectra. The solid-curves were the best fits of equation (1) to the experimental data by a nonlinear squares method, affording values of $k_{obsd} = (7.7 \pm 0.2) \times 10^{-3}$ s^{-1} at 224 nm and $k_{obsd} = (8.3 \pm 0.2) \times 10^{-3}$ s^{-1} at 270 nm. Figure S3: pseudo-first-order rate constants k_{obsd} versus $[TGA]_{tot}$ in buffer solutions of different pHs at 25.0°C and $\mu = 1.0$ M. Figure S4: pseudo-first-order rate constants k_{obsd} versus $[TGA]_{tot}$ in buffer solutions of different pHs at 25.0°C and $\mu = 1.0$ M. Figure S5: mass spectrum obtained for a reaction mixture of 1 mM *cis*-$[Pt(NH_3)_4Cl_4]$ and 8 mM thioglycolic acid in 10 mM HCl after a reaction time about 1 h. Peak assignments: *m/z* 183.0 for $[HOOCCH_2S\text{-}SCH_2COOH]\cdot H^+$; *m/z* 205.0 for $[HOOCCH_2S\text{-}SCH_2COOH]\cdot Na^+$. Figure S6: mass spectrum obtained for a reaction mixture of 1 mM *cis*-$[Pt(NH_3)_4Cl_4]$ and 8 mM thiolactic acid in 10 mM HCl after a reaction time about 1 h. Peak assignments: *m/z* 211.0 for [HOOCCH(Me) S-SCH(Me)COOH]·H^+; *m/z* 233.0 for [HOOCCH(Me)S-SCH(Me)COOH]·Na^+; *m/z* 249.0 for [HOOCCH(Me)S-SCH(Me)COOH]·K^+. Figure S7 (upper panel): TGA species *versus* pH distribution diagram at 25.0°C which was calculated by use of $pK_{a1} = 3.52$ and $pK_{a2} = 10.05$. Lower panel: reactivity of the TGA species *versus* pH distribution diagram in the reduction of *cis*-$[Pt(NH_3)_2Cl_4]$; the above pK_a values and $k_1 = 0.26$, $k_1 = 6.85$, and $k_4 = 1.15 \times 10^6$ $M^{-1}s^{-1}$ in Table 1 were employed in the calculation. Species **I** = $HSCH_2COOH$; **II** = $HSCH_2COO^-$; **III** = $^-SCH_2COO^-$. Figure S8 (upper panel): TLA species *versus* pH distribution diagram at 25.0°C which was calculated by use of $pK_{a1} = 3.38$ and $pK_{a2} = 9.93$. Lower panel: reactivity of the TLA species *versus* pH distribution diagram in the reduction of *cis*-$[Pt(NH_3)_2Cl_4]$; the above pK_a values and $k_1 = 0.19$, $k_1 = 6.2$, and $k_4 = 8.8 \times 10^8$ $M^{-1}s^{-1}$ in Table 1 were employed in the calculation. Species **I** = HSCHMeCOOH; **II** = $HSCHMeCOO^-$; **III** = –SCHMeCOO–. Figure S9 (upper panel): species of coenzyme M *versus* pH distribution diagram at 25.0°C which was calculated by use of $pK_{a1} = 1.65$ (assumed) and $pK_{a2} = 8.85$. Lower panel: reactivity of the coenzyme M species *versus* pH distribution diagram in the reduction process of *cis*-$[Pt(NH_3)_2Cl_4]$; the above pK_a values and $k_1 = 0$, $k_1 = 37$, and $k_4 = 3.29 \times 10^5$ $M^{-1}s^{-1}$ in Table 1 were employed in the calculation. Species **I** = $HSCH_2CH_2SO_3H$; **II** = $HSCH_2CH_2SO_3^-$; **III** = $^-SCH_2$ $CH_2SO_3^-$. (*Supplementary Materials*)

References

[1] M. H. Cohen, R. Dagher, D. J. Griebel et al., "U.S. Food and drug administration drug approval summaries: imatinib mesylate, mesna tablets, and zoledronic acid," *The Oncologist*, vol. 7, no. 5, pp. 393–400, 2002.

[2] M. Links and C. Lewis, "Chemoprotectants. a review of their clinical pharmacology and therapeutic efficacy," *Drugs*, vol. 57, no. 3, pp. 239–308, 1999.

[3] A. K. Souid, R. C. Fahey, M. K. Aktas et al., "Blood thiols following amifostine and Mesna infusions, a pediatric oncology group study," *Drug Metabolism & Disposition*, vol. 29, no. 11, pp. 1460–1466, 2001.

[4] W. E. Balch and R. S. Wolfe, "Specificity and biological distribution of coenzyme M (2-mercaptoethanesulfonic acid)," *Journal of Bacteriology*, vol. 137, no. 1, pp. 256–263, 1979.

[5] J. R. Allen, D. D. Clark, J. G. Krum, and S. A. Ensign, "A role for coenzyme M (2-mercaptoethanesulfonic acid) in a bacterial pathway of aliphatic epoxide carboxylation," *Proceedings of the National Academy of Sciences*, vol. 96, no. 15, pp. 8432–8437, 1999.

[6] A. M. Krishnakumar, D. Sliwa, J. A. Endrizzi, E. S. Boyd, S. A. Ensign, and J. W. Peters, "Getting a handle on the role of coenzyme M in alkene metabolism," *Microbiology and Molecular Biology Reviews*, vol. 72, no. 3, pp. 445–456, 2008.

[7] R. Laso-Pérez, G. Wegener, K. Knittel et al., "Thermophilic archaea activate butane via alkyl-coenzyme M formation," *Nature*, vol. 539, no. 7629, pp. 396–401, 2016.

[8] D. Criri, M. G. Fabbrini, A. Pratesi et al., "The leading established metal-based drugs: a revisitation of their relevant physico-chemical data," *Biometals*, vol. 32, no. 5, pp. 813–817, 2019.

[9] K. M. Deo, D. L. Ang, B. McGhie et al., "Platinum coordination compounds with potent anticancer activity," *Coordination Chemistry Reviews*, vol. 375, pp. 148–163, 2018.

[10] R. Oun, Y. E. Moussa, and N. J. Wheate, "The side effects of platinum-based chemotherapy drugs: a review for chemists," *Dalton Transactions*, vol. 47, no. 19, pp. 6645–6653, 2018.

[11] Y. Liu, H. Tian, L. Xu et al., "Investigations of the kinetics and mechanism of reduction of a carboplatin Pt(IV) prodrug by the major small-molecule reductants in human plasma," *International Journal of Molecular Sciences*, vol. 20, no. 22, p. 5660, 2019.

[12] M. Satoh, N. Kashihara, S. Fujimoto et al., "A novel free radical scavenger, edarabone, protects against cisplatin-induced acute renal damage in vitro and in vivo," *Journal of Pharmacology and Experimental Therapeutics*, vol. 305, no. 3, pp. 1183–1190, 2003.

[13] D. G. Sar, M. Montes-Bayon, E. B. Gonzalez, L. M. S. Zapico, and A. Sanz-Medel, "Reduction of cisplatin-induced nephrotoxicity in vivo by selenomethionine: the effect on Cisplatin-DNA adducts," *Chemical Research in Toxicology*, vol. 24, no. 6, pp. 896–904, 2011.

[14] P. R. Brock, K. P. Knight, D. R. Freyer et al., "Platinum-induced ototoxicity in children: a consensus review on mechanisms, predisposition, and protection, including a new international society of pediatric oncology Boston ototoxicity scale," *Journal of Clinical Oncology*, vol. 30, no. 19, pp. 2408–2417, 2012.

[15] A. Najjar, N. Rajabi, and R. Karaman, "Recent approaches to platinum(IV) prodrugs: a variety of strategies for enhanced delivery and efficacy," *Current Pharmaceutical Design*, vol. 23, no. 15, pp. 2366–2376, 2017.

[16] E. Petruzzella, R. Sirota, I. Solazzo, V. Gandin, and D. Gibson, "Triple action Pt(iv) derivatives of cisplatin: a new class of potent anticancer agents that overcome resistance," *Chemical Science*, vol. 9, no. 18, pp. 4299–4307, 2018.

[17] S. Q. Yap, C. F. Chin, A. H. Hong Thng, Y. Y. Pang, H. K. Ho, and W. H. Ang, "Finely tuned asymmetric platinum(IV) anticancer complexes: structure-activity relationship and application as orally available prodrugs," *ChemMedChem*, vol. 12, no. 4, pp. 300–311, 2017.

[18] D. Tolan, V. Gandin, L. Mprrison et al., "Oxidative stress Induced by Pt(IV) pro-drugs based on the cisplatin scaffold and indole carboxylic acids in axial position," *Scientific Reports*, vol. 6, p. 29367, 2016.

[19] K. Ormstad, S. Orrenius, T. Låstbom et al., "Pharmacokinetics and metabolism of sodium 2-mercaptoethanesulfonate in the rat," *Cancer Research*, vol. 43, no. 1, pp. 333–338, 1983.

[20] S. G. Allan, J. F. Smyth, F. G. Hay, R. C. Leonard, and C. R. Wolf, "Protective effect of sodium-2-mercaptoethanesulfonate on the gastrointestinal toxicity and lethality of cis-diamminedichloroplatinum," *Cancer Research*, vol. 46, no. 7, pp. 3569–3573, 1986.

[21] O. R. Leeuwenkamp, J. P. Neijt, W. J. van der Vijgh, and H. M. Pinedo, "Reaction kinetics of cisplatin and its monoaquated species with the modulating agents (di)mesna and thiosulphate," *European Journal of Cancer (Oxford, England : 1990)*, vol. 27, no. 10, pp. 1243–1247, 1991.

[22] J. Yeh, B. S. Kim, and J. Peresie, "Protection against cisplatin-induced ovarian damage by the antioxidant sodium 2-mercaptoethanesulfonate (mesna) in female rats," *American Journal of Obstetrics Gynecology*, vol. 198, no. 4, pp. 463.e1–463.e7, 2008.

[23] X. Li, S. Yang, X. Lv et al., "The mechanism of mesna in protection from cisplatin-induced ovarian damage in female rats," *Journal of Gynecologic and Oncology*, vol. 24, no. 2, pp. 177–185, 2013.

[24] C. E. Araujo, J. C. Cervellino, C. Pirisi, O. Pannunzio, and J. Callegari, "Chemotherapy with high dose ifosfamide/mesna plus cisplatin for the treatment of ovarian cancer: a study of the Grupo de Estudio y Tratamiento Latino-Americano del cancer," *Journal of Surgical Oncology*, vol. 46, no. 3, pp. 198–202, 1991.

[25] C. Vallejos, A. Solidoro, H. Gómez et al., "Ifosfamide plus cisplatin as primary chemotherapy of advanced ovarian cancer," *Gynecologic Oncology*, vol. 67, no. 2, pp. 168–171, 1997.

[26] C. A. Papadimitrou, C. Kouroussi, L. A. Moulopoulos et al., "Ifosfamide, paclitaxel and cisplatin first-line chemotherapy in advanced, suboptimally debulked epithelial ovarian cancer," *Cancer*, vol. 92, no. 7, pp. 1856–1863, 2001.

[27] A. Oprea, H. Bazzazi, B. Kangarloo, and J. R. A. Wolff, "The kinetics and mechanisms of the reaction of Mesna with cisplatin, oxiplatin and carboplatin," *Anticancer Research*, vol. 21, no. 2A, pp. 1225–1229, 2001.

[28] R. A. Adigun, M. Mhike, W. Mbiya, S. B. Jonnalagadda, and R. H. Simoyi, "Oxyhalogen-sulfur chemistry: kinetics and mechanism of oxidation of chemoprotectant, sodium 2-mercaptoethanesulfonate, Mesna, by acidic bromate and aqueous bromine," *The Journal of Physical Chemistry A*, vol. 118, no. 12, pp. 2196–2208, 2014.

[29] R. A. Adigun, B. Martincigh, V. O. Nyamori, B. Omondi, C. Masimirembwa, and R. H. Simoyi, "Kinetics and mechanistic investigation into the possible activation of imidazolium trans-[tetra-chloridodimethylsulfoxideimidazoleruthenate(iii)], NAMI-A, by 2-mercaptoethane sulfonate," *Dalton Transactions*, vol. 43, no. 34, pp. 12943–12951, 2014.

[30] M. C. McCormick, K. Keijzer, A. Polavarapu, F. A. Schultz, and M.-H. Baik, "Understanding intrinsically irreversible, non-nernstian, two-electron redox processes: a combined experimental and computational study of the electrochemical activation of platinum(IV) antitumor prodrugs," *Journal of the American Chemical Society*, vol. 136, no. 25, pp. 8992–9000, 2014.

[31] M. D. Hall, H. L. Daly, J. Z. Zhang et al., "Quantitative measurement of the reduction of platinum(IV) complexes using X-ray absorption near-edge spectroscopy (XANES)," *Metallomics*, vol. 4, no. 6, pp. 568–575, 2012.

[32] J. Dong, Y. Ren, S. Huo et al., "Reduction of ormaplatin and *cis*-diamminetetrachloroplatinum(IV) by ascorbic acid and dominant thiols in human plasma: kinetic and mechanistic analyses," *Dalton Transactions*, vol. 45, no. 28, pp. 11326–11337, 2016.

[33] H. Tian, J. Dong, X. Chi, L. Xu, H. Shi, and T. Shi, "Reduction of cisplatin and carboplatin Pt(IV) prodrugs by homocysteine: kinetic and mechanistic investigations," *International Journal of Chemical Kinetics*, vol. 49, no. 9, pp. 681–689, 2017.

[34] X. Zhang, "Oxidations of benzhydrazide and phenylacetic hydrazide by hexachloroiridate(IV): reaction mechanism and structure-reactivity relationship," *Molecules*, vol. 25, no. 2, p. 308, 2020.

[35] S. Jovanovic, B. Petrovic, and Z. D. Bugarcic, "The UV-VIS, HPLC and 1H NMR studies of the substitution reactions of some Pt(IV) complexes with 5'-GMP and L-histidine," *Journal of Coordination Chemistry*, vol. 63, no. 14–16, pp. 2419–2430, 2010.

[36] M. Arsenijevic, M. Milovanovic, V. Volarevic et al., "Cytotoxic properties of platinum(IV) and dinuclear platinum(II) complexes and their ligand substitution reactions with guanosine-5′-monophosphate," *Transition Metal Chemistry*, vol. 37, no. 12, pp. 481–488, 2012.

[37] T. Shi, J. Berglund, and L. I. Elding, "Kinetics and mechanism for reduction oftrans-dichlorotetracyanoplatinate(IV) by thioglycolic acid,l-cysteine,dl-penicillamine, and glutathione in aqueous solution," *Inorganic Chemistry*, vol. 35, no. 12, pp. 3498–3503, 1996.

[38] A. Chipman, B. F. Yates, A. J. Canty, and A. Ariafard, "Reduction of a platinum(iv) prodrug model by sulfur containing biological reductants: computational mechanistic elucidation," *Chemical Communications*, vol. 54, no. 74, pp. 10491–10494, 2018.

[39] J. Wang, H. Yao, T. Lu et al., "Spectroscopic, kinetic, and theoretical analyses of oxidation of dl-ethionine by Pt(IV) anticancer model compounds," *Spectrochimica Acta Part A: Molecular and Biomolecular Spectroscopy*, vol. 223, p. 117328, 2019.

[40] A. E. Martell and R. M. Smith, "Critical stability constants," *Other Organic Ligands*, Plenum Press, vol. 3, p. 75, New York, NY, USA, 1975.

[41] B. L. Urquhart, A. A. House, M. J. Cutler, J. D. Spence, and D. J. Freeman, "Thiol exchange: an in vitro assay that predicts the efficacy of novel homocysteine lowering therapies," *Journal of Pharmaceutical Sciences*, vol. 95, no. 8, pp. 1742–1750, 2006.

[42] A. K. Covington and R. Thompson, "Ionization of moderately strong acids in aqueous solution. Part III. Methane-, ethane-, and propanesulfonic acids at 25°C," *Journal of Solution Chemistry*, vol. 3, no. 8, pp. 603–617, 1974.

[43] C. Cabrele, S. Fiori, S. Pegoraro, and L. Moroder, "Redox-active cyclic bis(cysteinyl)peptides as catalysts for in vitro oxidative protein folding," *Chemistry & Biology*, vol. 9, no. 6, pp. 731–740, 2002.

[44] S. Huo, S. Shen, D. Liu, and T. Shi, "Oxidation of 3,6-dioxa-1,8-octanedithiol by platinum(IV) anticancer prodrug and model complex: kinetic and mechanistic studies," *The Journal of Physical Chemistry B*, vol. 116, no. 22, pp. 6522–6528, 2012.

[45] H. Yao, H. Tian, L. Xu et al., "Kinetic and mechanistic analysis of oxidation of 2-furoic hydrazide by hexachloroirradate(IV) in a wide pH range," *Transition Metal Chemistry*, vol. 44, no. 8, pp. 771–777, 2019.

[46] C. Nan, J. Dong, H. Tian et al., "Oxidations of hydrazine and substituted hydrazines by hexachloroiridate(IV) in aqueous solution: kinetic and mechanistic analyses," *Journal of Molecular Liquids*, vol. 256, pp. 489–496, 2018.

[47] C. Liu, L. Xu, H. Tian, H. Yao, L. I. Elding, and T. Shi, "Kinetics and mechanism for reduction of Pt(IV) anticancer model compounds by Se-methyl L-selenocysteine. Comparison with L-selenomethionine," *Journal of Molecular Liquids*, vol. 271, pp. 838–843, 2018.

[48] T. Shi and L. I. Elding, "Kinetics and mechanism for reduction of trans-dichloro-tetracyanoplatinate(IV) by tetraammine-platinum(II) and bis(ethylenediamine)platinum(II)," *Inorganica Chimica Acta*, vol. 282, pp. 55–60, 1998.